Mechanical Consequences of Molecular Composition on Failure in Polyolefin Composites Containing Glassy, Elastomeric, and Semicrystalline Components

Mahesh K. Mahanthappa,[†,‡,§] Marc A. Hillmyer,[†] and Frank S. Bates*[,‡]

Department of Chemical Engineering and Materials Science and Department of Chemistry, University of Minnesota, Minneapolis, Minnesota 55455

Received May 27, 2007; Revised Manuscript Received December 1, 2007

ABSTRACT: In order to gain insights into the mechanisms of deformation and ultimate failure in a homologous series of lamellae-forming polyolefin block copolymers comprised of glassy poly(cyclohexylethylene) (C), elastomeric poly(ethylene-*alt*-propylene) (P), and semicrystalline poly(ethylene) (E), the anisotropic tensile properties of samples in which the microphase separate structure is oriented on a macroscopic length scale were probed. Reciprocating shear processing of monodisperse CPCPC and CPEPC-ξ polymers having mass fraction $w_C \sim 0.39-0.44$ and $0 \leq \xi \leq 1$, where $\xi = w_E/(w_E + w_P)$, produces "single-grain" polymer samples with perpendicular-oriented lamellae. Tensile deformation studies in which the strain axis coincides with the lamellar normal direction yield varied mechanical responses ranging from brittle fracture for CEC ($\xi = 0$) to ductile behavior for CPEPC ($\xi > 0$) and CPCPC. Tandem small- and wide-angle X-ray scattering analysis of samples undergoing deformation shows that application of strain along the lamellar normal in the CPEPC materials results in formation of a folded lamellar structure or "chevron" morpohology within which the E crystals cant relative to the strain direction. Since the ultimate failure mechanism for materials strained in this direction is chain pullout in the glassy domains, a simple mechanical model applied to the data enables quantitation of the stress required for chain pullout at ~4 MPa. Additionally, the mechanical properties of miscible blends of CEC and CPC polymers with matched segregation strengths are shown to mimic those of the covalently linked CPEPC pentablock copolymer.

Introduction

Multiblock copolymers exhibit a composite mechanical response that depends sensitively upon their constituent homopolymer segments, the molecular architecture, and the chain topology.[1−5] Linear multiblock copolymers that incorporate glassy, semicrystalline, and rubbery homopolymer segments in a pairwise fashion are the most well-studied members of this class of technologically useful materials. Numerous investigations of polydomain and "single-grain" block copolymer samples have demonstrated that linear polymers with glassy end blocks having either rubbery or semicrystalline blocks in the middle of the chain display a high degree of mechanical strength at relatively low molecular weights.[3,6−10] Styrenic block copolymers containing rubbery poly(butadiene) (B) or poly(isoprene) (I) segments are among the most common block copolymer plastics and thermoplastic elastomers. In the former case, glassy poly(styrene) (S) domains form the matrix phase within which the B or I domains are dispersed, resulting in increased compliance and impact strength as exemplified by the commercially available K-resins.[11] Conversely, diene-rich $(SI)_n$ or $(SB)_n$ multiblock polymers are commodity thermoplastic elastomers, in which the dispersed S domains (typically, hexagonally packed cylinders or body-centered cubic spheres) serve as physical cross-links within a rubbery diene matrix.[1]

Mechanical processing of neat block copolymer melts under controlled conditions yields "single-domain" or "single crystal" monolithic materials, in which the microphase separated morphology is preferentially oriented over macroscopic length scales.[12−14] Investigations of the shear processing of multiblock copolymers under a variety of conditions and experimental geometries have furnished a phenomenological understanding of the parameters that dictate the orientation of the underlying microphase separated structure, especially in the case of ABA-type triblock copolymers. As a consequence of the oriented microphase-separated structure, these materials exhibit a composite mechanical response that depends delicately upon the relative sizes and arrangements of the constituent polymer blocks. The mechanical properties of oriented glassy−rubbery and glassy−semicrystalline cylinder- and lamellar-forming materials have been the subject of multiple investigations and have been previously reviewed.[15]

Studies of the uniaxial tensile deformation of "single crystal" SBS materials in conjunction with small-angle X-ray scattering (SAXS) and transmission electron microscopy (TEM) afforded fundamental insights into the morphological transformations that these materials undergo during deformation.[9,10] Synchrotron SAXS measurements of lamellar SBS triblocks undergoing uniaxial elongation established that the microphase separated structure undergoes buckling and grain rotation while maintaining a near constant layer spacing to form a "chevron" morphology. Real-space TEM images of samples stained in tension indicate that the layers break to form wavy lamellae. At large strains, the mechanical properties reflect the effects of chain deformation and reorientation by the applied tensile load. Read et al. developed a theoretical model for the deformation of microphase separated lamellae along the lamellar normal that establishes that chevron formation occurs at a critical strain due to mechanical instability in the layers.[16] By using constituitive

* To whom correspondence should be addressed. E-mail: bates@cems.umn.edu.
[†] Department of Chemistry.
[‡] Department of Chemical Engineering and Materials Science.
[§] Current address: Department of Chemistry, 1101 University Ave., University of Wisconsin, Madison, WI 53706.

10.1021/ma071196r CCC: $40.75
Published on Web 02/02/2008

Table 1. Characterization Data for Polydomain CPEPC,[a] CECCPC-50, and CPCPC Block Copolymers

sample	M_n (kg mol^{-1})	M_w/M_n[b]	w_C	w_P	w_E	T_{ODT} (°C)[d]	d (nm)[e]	$T_{m,E}$ (°C)[f]	X_c (%)[g]	overall E cryst (%)
CEC	29.8	1.02	0.424	0	0.576	217	20.8	94.2	17.7	10.2
CPEPC-70	30.7	1.15	0.411	0.178	0.411	236	21.6	93.7	24.5	10.1
CPEPC-50	20.9	1.11	0.441	0.281	0.278	208	20.0	92.8	31.6	8.8
CPEPC-30	38.6	1.12	0.394	0.423	0.183	237	22.3	84.5	39.8	7.3
CPC	46.1	(1.03)[c]	0.395	0.605	0	234	22.9	n.a.	0	0
CEC/CPC-50	n.a.	n.a.	0.410	0.302	0.288	225	22.0	94.2	31.1	9.0
CPCPC	76.0	1.05	0.464	0.536	0	225	22.1	n.a.	0	0

[a] Data taken from ref 28. [b] Determined by size exclusion chromatography (SEC) with poly(styrene) calibration standards in trichlorobenzene at 135 °C. [c] Measured for the unsaturated precursor by SEC in tetrahydrofuran at 25 °C. [d] Measured by dynamic mechanical spectroscopy. [e] Measured by synchrotron SAXS at 150 °C. [f] Peak melting temperature of the poly(ethylene) (E) block determined by DSC. [g] Percent crystallinity in the E block.

properties of the material, such as the bending and tensile moduli of the parent homopolymers, this model quantitatively predicts the strain at which layer buckling occurs. Similar phenomena have been observed in rubbery−semicrystalline EPE triblocks (E = poly(ethylene) and P = poly(ethylene-*alt*-propylene)).[17]

With the advent of efficient heterogeneous catalysts capable of completely hydrogenating poly(styrene) (>99% saturated), poly(cyclohexylethylene) (C) has emerged as a new engineering thermoplastic that exhibits a higher upper use temperature T_g = 147 °C compared to its parent poly(styrene).[18] C-based polymers exhibit a higher degree of chemical, thermal, and photochemical stability due to the elimination of potentially reactive functionalities in the polymer backbone through an inexpensive, single-step postsynthetic modification reaction.[19] Catalytic hydrogenation of conventional SBS block copolymers, with varying terminal vinyl content in the center B block, yields C/E glassy−semicrystalline resins with varying degrees of crystallinity that exhibit a continuum of properties from plastics to elastomers that eclipse those of traditional thermoplastic elastomers.[20] For this reason, the phase behavior of these new materials has been studied extensively along with their attendant processability and mechanical properties.[4,5,21−29]

Hermel et al. investigated the mechanical behavior of shear processed glassy−semicrystalline CEC and CECEC block copolymers.[4] Application of strain along the lamellar normal of a shear oriented CEC block copolymer led to brittle fracture at low strains due to chain pullout in the C domains. In contrast to the brittle behavior of the aligned CEC, application of strain along the lamellar normal to aligned CECEC pentablock copolymers resulted in chevron formation while maintaining a constant domain spacing. Ultimate failure at high strains by chain pullout in the C domain was presumed to be the dominant mode of failure in the pentablock materials.

Recently, we reported the synthesis and characterization of a homologous series of CPEPC pentablock copolymers that incorporate glassy C, rubbery P, and semicrystalline E blocks.[28] At a fixed glass content ($f_C \sim 0.4$), the mechanical properties of these materials depend sensitively on the relative amounts of E and P present. Increasing the E content causes monotonic increases in the elastic modulus E and yield stress σ_{yield} with decreasing failure strains ϵ_{fail}. Therefore, the effect of the semicrystalline E is similar to the addition of a brittle filler to a triblock copolymer elastomer. In this contribution, we examine the effects of shear processing on the microstructure and mechanical response of these CPEPC materials. We demonstrate that the incorporation of a short rubbery segment dramatically mitigates the brittleness of the aligned CEC triblocks. Additionally, we demonstrate that a mechanical response comparable to that of the CPEPC materials can be achieved by blending judiciously synthesized CEC and CPC triblock copolymers.

Scheme 1

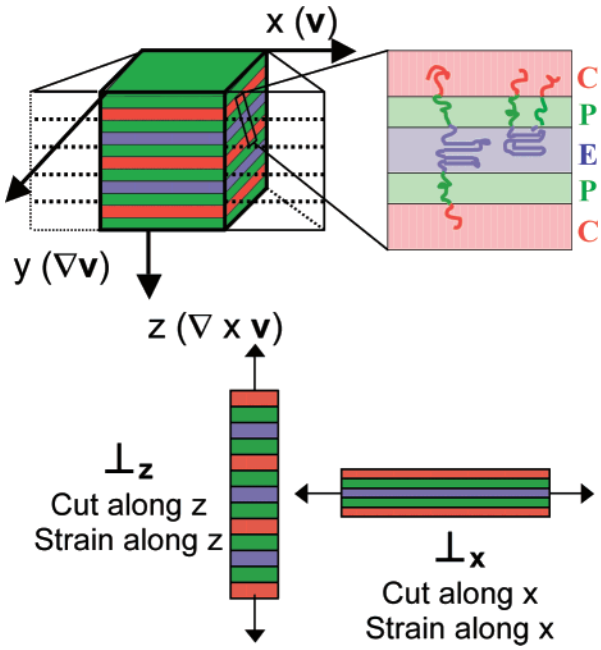

Experimental Section

Materials. CPEPC block copolymers were synthesized by sequential anionic polymerization of styrene, isoprene, and butadiene followed by heterogeneous catalytic hydrogenation. Details of the synthesis and characterization of these materials have been reported elsewhere,[28] and relevant molecular characterization data from the previous report are summarized in Table 1. Samples are named according to the previously established nomenclature: the letters specify the block sequence with C, P, and E corresponding to poly(cyclohexylethylene), poly(ethylene-*alt*-propylene), and poly(ethylene), and the number indicates the value of 100ξ, where $\xi = w_E/(w_E + w_P)$. For example, CPEPC-50 refers to a sample with $w_E = w_P$ and $w_C \sim 0.4$. The poly(ethylene) (E) segments contain 21 ethyl branches per 1000 carbon atoms, and the poly(ethylene-*alt*-propylene) (P) segments contain 15 isopropyl branches per 1000 carbon atoms.

A CPCPC block copolymer was synthesized by an analogous procedure: Sequential anionic polymerization of styrene and isoprene in cyclohexane at 40 °C under anaerobic and anhydrous conditions yields a SISIS block copolymer. Subsequent catalytic hydrogenation of this pentablock copolymer over a Pt/Re/SiO_2 catalyst[18] yielded the desired CPCPC block copolymer, with greater than 97% saturation of the polymer assessed by ^{1}H NMR spectroscopy at 100 °C in d_2-tetrachloroethane. The molecular parameters of this sample are also given in Table 1.

Thermal Analysis. Differential scanning calorimetry was performed on a TA Instruments Q1000 DSC using the previously reported protocol: Each sample was heated to 150 °C for 10 min to erase thermal history before cooling it to − 80 °C at 5 °C/min. Heat flow vs temperature curves were then acquired by heating

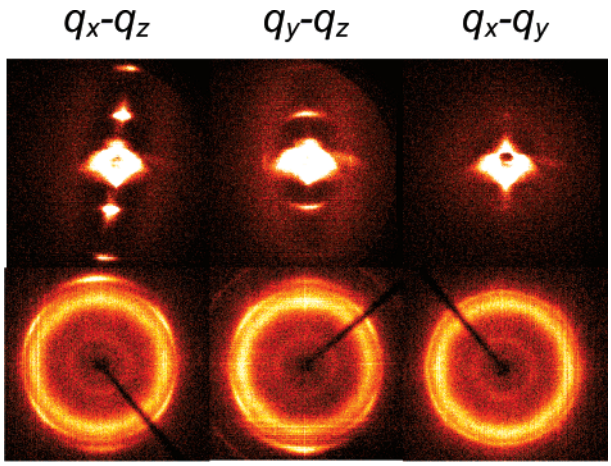

Figure 1. Representative SAXS (top) and WAXS (bottom) patterns of CPEPC-50 processed by reciprocating shear alignment taken with the X-ray beam incident upon the q_x-q_z, q_y-q_z, and q_x-q_y planes, indicating the "perpendicular" alignment of the lamellae relative to the velocity direction (x).

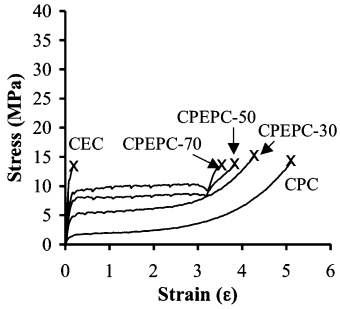

Figure 2. Representative stress (σ) vs strain (ϵ) curves for $\perp_z$ samples.

the sample at rate of 5 °C/min from −80 to 150 °C. From this data, E block crystallinity X_c of the samples was calculated as

$$X_c = \Delta H_m / w_E \Delta H^\circ_{m,E}$$

where $\Delta H^\circ_{m,E} = 277$ J/g is the theoretical heat of melting for perfectly crystalline polyethylene.[30]

Dynamic Mechanical Spectroscopy. Dynamic mechanical spectroscopy[31,32] was used to locate the block copolymer order−disorder phase transition temperatures (T_{ODT}), using a Rheometric Scientific ARES strain-controlled rheometer fitted with 25 mm diameter parallel plates. Dynamic strain sweep measurements conducted at 140 °C established that strains $|\gamma| = 0.5-1\%$ provided a linear viscoelastic response. In isochronal temperature ramp tests conducted in the linear viscoelastic regime using a heating rate of 2 °C/min, a cooling rate of 5 °C/min, a frequency of $\omega = 1$ rad/s, and a strain $|\gamma| = 1\%$, the dynamic elastic storage shear modulus (G') was measured as a function of temperature. G' drops precipitously as the microphase-separated material undergoes a first-order phase transition to the disordered polymer melt at T_{ODT}. Isothermal frequency sweeps conducted with $100 \le \omega \le 0.01$ rad/s and $|\gamma| = 0.5-1\%$ at several temperatures confirmed the location of T_{ODT}.

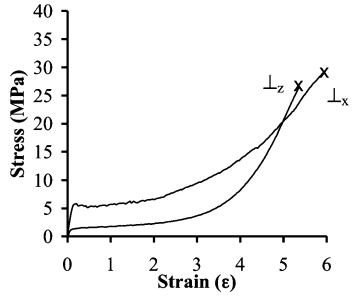

Figure 3. Representative stress (σ) vs strain (ϵ) curves for CPCPC $\perp_x$ and $\perp_z$.

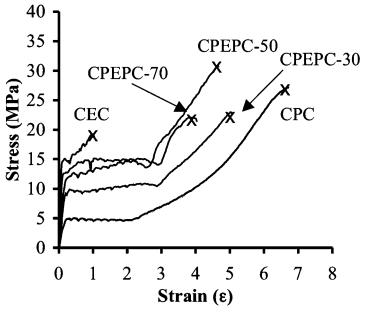

Figure 4. Representative stress (σ) vs strain (ϵ) curves for $\perp_x$ samples.

SAXS. Synchrotron small-angle X-ray scattering (SAXS) measurements were performed at the 5IDD beamline of the DuPont-Northwestern-Dow Collaborative Access Team Synchrotron Research Center at the Advanced Photon Source (Argonne, IL). Two-dimensional SAXS patterns were acquired on a MAR-CCD detector (133 mm diameter active circular area) with 2048 × 2048 pixel resolution using a beam energy of 8 keV ($\lambda = 1.54$ Å) and a 3.026 m sample-to-detector distance. Samples were heated to T_{ODT} + 10 °C (see Table 1) for 5 min to disorder the melt and erase thermal history, cooled to 150 °C at 10 °C/min, and held at 150 °C for 5 min before data collection (typical exposure times ∼ 20 s). Samples were subsequently cooled to 25 °C at 10 °C/min, and a SAXS pattern was taken after a 5 min equilibration period.

Laboratory source SAXS measurements were performed in the Characterization Facility of the Institute of Technology at the University of Minnesota. Cu Kα X-rays from a Rigaku RU-200VBH rotating anode were collimated using two Osmic, Inc. Max-Flux multilayer confocal mirrors. Passage of the resulting X-ray beam through three pinhole apertures trimmed the final beam diameter to 0.5 mm. Samples were mounted in a helium-purged sample chamber. 2D-SAXS data were acquired on a Siemens Hi-STAR area detector with a 3.53 m sample-to-detector distance.

WAXS. A Bruker AXS microdiffractometer was used to acquire two-dimensional wide-angle X-ray scattering (WAXS) patterns in transmission mode. Experiments employed Cu Kα X-rays generated from a 4XE short anode, monochromated using flat graphite, and collimated through two 0.8 mm pinholes with a sample-to-detector distance of 5.92 cm.

Polydomain Tensile Sample Preparation. Polymer films were produced by compression-molding between Teflon sheets at $T = T_{ODT}$ + 10 °C for 10 min at 14.0 MPa, followed by cooling to

Table 2. Ultimate Properties of Shear-Aligned $\perp_z$ Block Copolymer Tensile Samples

sample	E (MPa)[a]	σ_{yield} (MPa)[b]	ϵ_{fail}[c]	σ_{fail} (MPa)[d]	chevron angle ϕ (deg)
CEC	141 ± 24	11.5 ± 1.4	0.24 ± 0.04	13.3 ± 0.4	n.a.
CPEPC-70	69.3 ± 5.3	9.2 ± 0.4	3.52 ± 0.33	13.3 ± 2.3	76
CPEPC-50	54.1 ± 2.3	7.5 ± 0.4	3.72 ± 0.13	13.3 ± 0.9	76
CPEPC-30	44.4 ± 2.1	5.3 ± 0.3	4.27 ± 0.23	14.8 ± 1.9	78
CPC	12.5 ± 3.1	1.4 ± 0.2	5.21 ± 0.30	14.4 ± 2.4	79.5
CEC/CPC-50	48.4 ± 2.7	6.3 ± 0.3	3.87 ± 0.14	19.1 ± 1.5	n.d.[e]
CPCPC	24.8 ± 6.8	1.8 ± 0.1	5.17 ± 0.24	21.1 ± 2.6	78

[a] E = elastic modulus. [b] σ_{yield} = engineering stress at yield. [c] ϵ_{fail} = elongation at failure. [d] σ_{fail} = engineering stress at failure. [e] Not determined.

Table 3. Ultimate Properties of Shear-Aligned $\perp_x$ Block Copolymer Tensile Samples

sample	E (MPa)[a]	σ_{yield} (MPa)[b]	ϵ_{fail} (MPa)[c]	σ_{fail} (MPa)[d]
CEC	246 ± 37	15.1 ± 1.2	0.97 ± 0.19	19.3 ± 0.2
CPEPC-70	113 ± 13	11.8 ± 1.3	3.86 ± 0.29	21.8 ± 2.2
CPEPC-50	84 ± 8	11.0 ± 0.4	4.66 ± 0.46	28.9 ± 4.2
CPEPC-30	61 ± 3	9.4 ± 0.4	5.19 ± 0.31	26.4 ± 3.0
CPC	33 ± 4	4.9 ± 0.4	6.57 ± 0.18	27.4 ± 4.7
CEC/CPC-50	n.d.	n.d.	n.d.	n.d.
CPCPC	34.4 ± 0.5	5.4 ± 0.2	5.56 ± 0.32	28.8 ± 3.5

[a] E = elastic modulus. [b] σ_{yield} = engineering stress at yield. [c] ϵ_{fail} = elongation at failure. [d] σ_{fail} = engineering stress at failure. [e] Not determined.

room temperature at 10 °C/min. In order to test the mechanical properties of the polydomain samples, a fresh razor blade was used to cut rectangular tensile bars measuring 15 mm × 2 mm × 1 mm from these films.

Flow-Induced Orientation. The parallel-plate reciprocating shear device previously described by Koppi et al.[12,13,33] was used to process compression-molded polymer films (1 mm thickness) under an argon atmosphere. Compression-molded films were placed in a channel measuring 50 mm × 20 mm between two brass plates situated 1 mm apart; the brass plates were covered with a heat-resistant aluminum tape to aid in recovery of the oriented samples. The shear from disorder protocol of Hermel et al. was used: the shear cell was heated to T_{ODT} + 10 °C for 10 min to disorder the polymer melt, after which application of shear commenced as the sample was cooled at a rate of 5 °C/min to T_{ODT} − 30 °C. A strain amplitude $|\gamma| = 2$ and period $t = 4$ s were employed, corresponding to a shear rate of 0.50 s^{-1}. Application of isothermal reciprocating shear for 45−60 min, followed by cessation of shear, and cooling to room temperature yielded macroscopically oriented block copolymer films as verified by SAXS. A fresh razor blade was used to cut rectangular tensile bars measuring 15 mm × 2 mm × 1 mm from these oriented films to produce $\perp_x$ and $\perp_z$ samples for tensile testing; Scheme 1 depicts the reciprocating shear alignment geometry and the associated directions along which tensile bars were cut.

Tensile Measurements. Uniaxial tensile tests were carried out at 22 °C using a Rheometrics Scientific MINIMAT operating with a cross-head speed of 5 mm/min (length-independent strain rate of 0.010 s^{-1}) using the aforementioned tensile bars with an initial gage length of 8 mm. Force−displacement measurements were converted to engineering stress $\sigma = F/A_0$ vs nominal strain $\epsilon = (l - l_0)/l_0$, where A_0 and l_0 are the initial cross-sectional area and length, respectively. The elastic modulus E of each sample was determined by linearly fitting the elastic portion of the stress−strain curve prior to yielding. Reported data reflect an average over a minimum of five independent trials unless otherwise specified.

"In situ" 2D-SAXS and 2D-WAXS patterns of samples undergoing tensile deformation were acquired using a modified MINIMAT holder that allowed the sample to be clamped at a fixed elongation, removed from the mechanical testing equipment, and analyzed with the X-ray beam incident on two faces of the tensile bar normal to the strain axis. Upon acquisition of a 2D-SAXS pattern (exposure times ∼ 120 s) or a 2D-WAXS pattern (exposure time ∼ 60 s), the sample was returned to the MINIMAT and elongated further.

Results and Analysis

Flow-Induced Alignment. Oriented "single-grain" samples of the CPEPC and CPCPC polyolefin block copolymers were produced by reciprocating shear processing. Scheme 1 illustrates the geometry of the shear alignment apparatus, in which **v** corresponds to the velocity (shear) x-direction, the shear gradient $\nabla\mathbf{v}$ is the y-direction, and the z-axis is the neutral direction ($\nabla\times\mathbf{v}$). In accord with previous reports on the flow-induced alignment of CEC and CECEC materials under reciprocating shear conditions, a single protocol achieved "perpendicular" alignment[14] in all of these materials, i.e., orientation of the planes of the microphase-separated lamellar structure perpendicular to the $\nabla\times\mathbf{v}$ direction. In order to reproducibly obtain this alignment condition, samples were first heated above the order−disorder transition temperature (T_{ODT} + 10 °C) for 10 min, at which time reciprocating shear commenced while cooling the samples to T_{ODT} − 30 °C at a rate of 5 °C/min. Cessation of shear after 1 h followed by cooling to room temperature furnished oriented samples. Representative 2-D SAXS patterns acquired with the X-ray beam incident on each of the three orthogonal faces of the aligned samples corroborates the perpendicular lamellar alignment (Figure 1). WAXS patterns taken with the X-ray beam directed along the same sample axes reveal that the E crystallites are oriented with the E chain axes parallel to the microphase-separated interfaces, as indicated by the four (110) scattering maxima and two meridonal (200) scattering peaks (Figure 1). This E crystal orientation has been previously observed in shear processed microphase-separated block copolymers, in which templated crystallization occurs within a microphase-separated melt.[17]

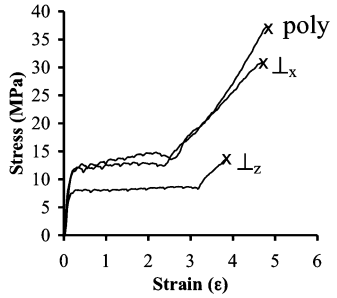

Figure 5. Representative stress (σ) vs strain (ϵ) curves for CPEPC $\perp_z$, CPEPC $\perp_x$, and polydomain samples.

Macroscopic Tensile Properties. According to the coordinate system in Scheme 1, tensile bars were cut from the shear processed samples for uniaxial tensile deformation experiments such that the strain axis coincides with (i) the z-axis ($\perp_z$) and (ii) the x-axis ($\perp_x$).

The $\perp_z$ CPEPC tensile bars exhibit varying degrees of ductility depending on the relative amounts of crystalline E and elastomeric P ($T_g \sim -60$ °C) present. Representative stress−strain curves for these samples are presented in Figure 2, and the average results over a minimum of five independent trials are provided in Table 2. Consistent with the results of Hermel et al.,[4] the $\perp_z$ CEC tensile samples are quite brittle and fracture at low strains ($\epsilon = 0.24$). (This failure strain is somewhat greater than that reported earlier for $\perp_z$ specimens, which we attribute to a lower C content.) The presence of even a short P block as in the CPEPC-70, however, dramatically alters the mechanical response of these materials such that they exhibit yielding, plastic deformation ("necking" or "cold drawing"), strain hardening, and ultimate failure. The elastic modulus (E) and the yield stress (σ_{yield}) increase with increasing E content, while the elongation at break (ϵ_{fail}) decreases. Samples having a high E content also exhibit a higher initial rate of strain hardening prior to failure. Notably, the $\perp_z$ tensile specimens break in the middle of the gage section and exhibit an ultimate engineering failure stress σ_{fail} that is nearly compositionally invariant over the homologous CPEPC series. Analogous to prior observations that the $\perp_z$ CECEC exhibits dramatically enhanced toughness compared to the $\perp_z$ CEC, $\perp_z$ CPCPC exhibits a much higher failure stress than the corresponding $\perp_z$ CPC (Figure 3). This behavior is likely a consequence of the ability of the CPCPC chain to mechanically couple up to five domains in the lamellar microphase-separated structure through a combination of "bridg-

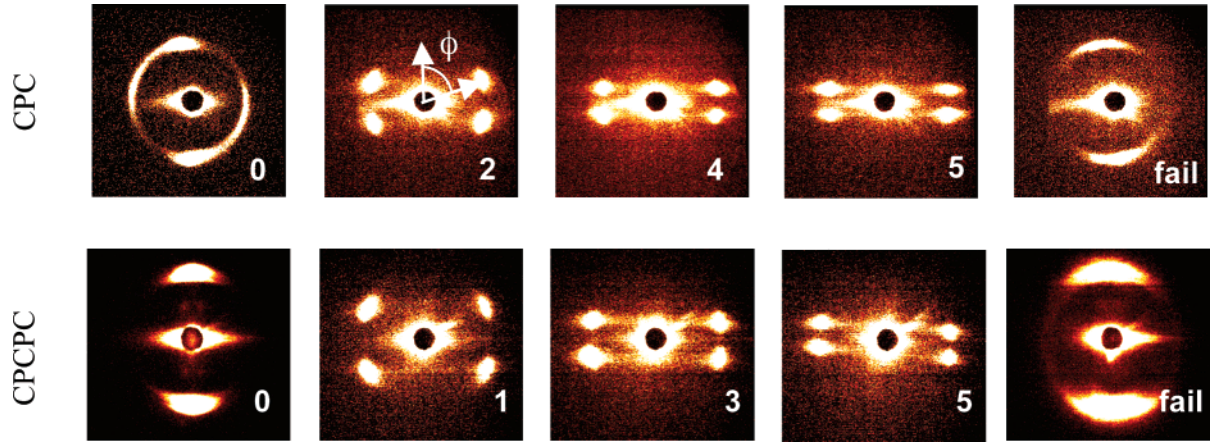

Figure 6. Representative "in situ" SAXS patterns taken with the X-ray beam incident on the q_y-q_z plane during tensile deformation of $\perp_z$ CPC and CPCPC samples at the indicated elongation (ϵ). Measurements reflect the structure in the necked region of the specimen. In the initial state ($\epsilon = 0$), the two oriented scattering maxima indicate the $\perp_z$ aligned lamellar morphology. Upon application of strain along the *z* direction (vertical), four new reflections appear at an angle ϕ (relative to the meridian) that depends upon the extent of elongation. Upon failure and recovery, the original two spot pattern is recovered.

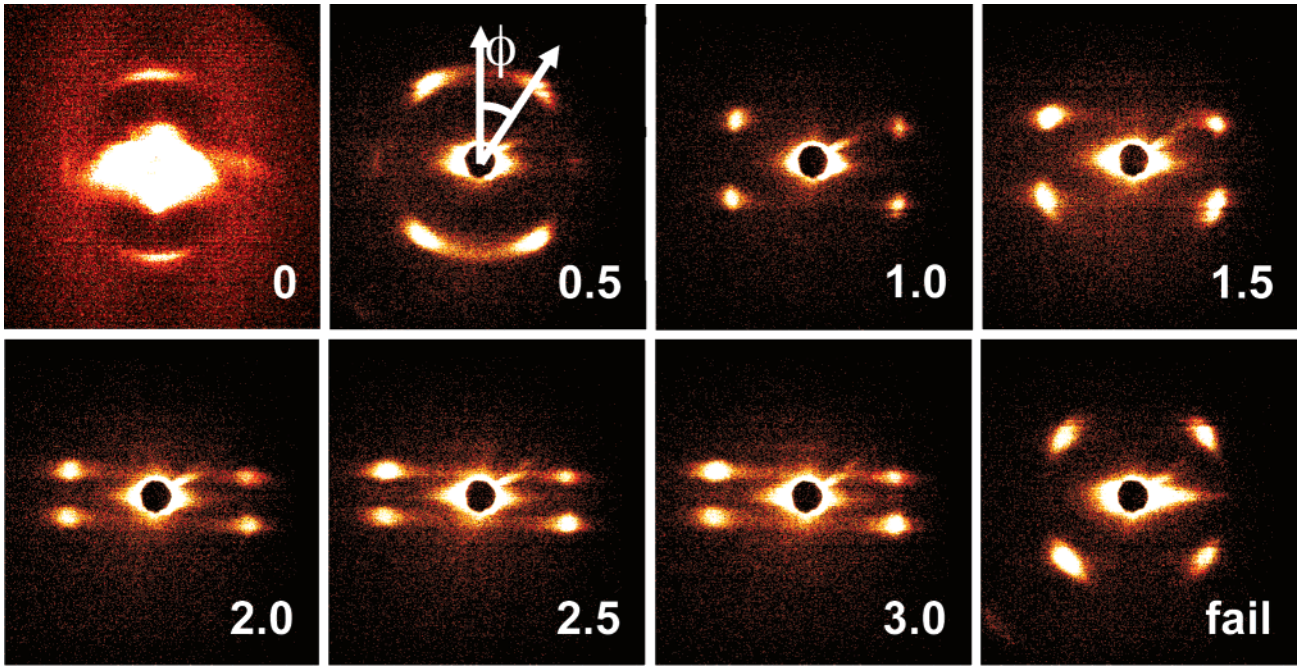

Figure 7. Representative "in situ" SAXS patterns taken with the X-ray beam incident on the sample neck in the q_y-q_z plane during tensile deformation of a $\perp_z$-CPEPC-50 sample at the indicated elongation (ϵ). Measurements reflect the structure in the necked region of the specimen. In the initial state ($\epsilon = 0$), the two oriented scattering maxima indicate the $\perp_z$-aligned lamellar morphology. Upon application of strain along the *z* direction (vertical), four new reflections appear at an angle ϕ (relative to the meridian) which depends upon the extent of elongation.

ing" and "looping" chain conformations as previously described by Bates and co-workers.[4,24,26,34,35]

Representative stress−strain curves for the $\perp_x$ CPEPC tensile samples are shown in Figure 4, and the corresponding average mechanical properties are provided in Table 3. As in the case of the $\perp_z$ CPEPC, the $\perp_x$ CPEPC samples exhibit monotonically increasing elastic moduli E and yield stresses σ_{yield} as the E content increases. While the failure strain ϵ_{fail} decreases with increasing E content, the failure stress σ_{fail} exhibits no obvious trend. Inconsistencies in σ_{fail} across the series of CPEPC materials are attributed to the observed uneven tearing of the samples into thin strands along the strain axis proceeded by failure in close proximity to the tensile grips. In contrast to the large observed difference in strength between the $\perp_z$ CPC and $\perp_z$ CPCPC, the properties of the CPC and CPCPC $\perp_x$ samples display no statistically significant variation.

A tensile data overlay for representative $\perp_z$, $\perp_x$, and polydomain CPEPC-50 samples is presented in Figure 5. Careful inspection of this figure shows that the polydomain sample, in which the microphase-separated lamellar grains are randomly oriented, exhibits a mechanical response similar to that of the $\perp_x$ sample, whereas the $\perp_z$ sample yields more readily, is substantially weaker, and does not strain harden appreciably.

Microstructural Investigations of $\perp_z$ Samples. In order to gain insights into the mechanism of deformation and the origins of the yielding behavior in the $\perp_z$ CPEPC materials, we undertook "in situ" SAXS analysis of samples undergoing uniaxial tensile deformation. Samples elongated in a MINIMAT tensile apparatus were clamped at fixed strains prior to failure and subjected to SAXS analyses along the two directions perpendicular to the strain direction (q_x-q_z and q_y-q_z). Figure 6 (upper panels) shows the results of "in situ" SAXS analysis

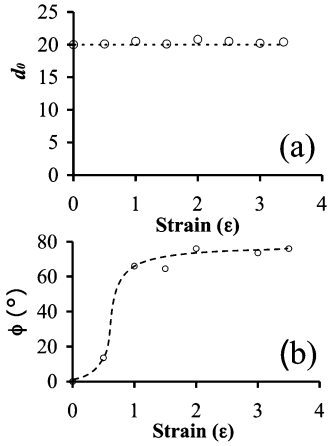

Figure 8. Dependence of (a) the principal domain spacing d_0 (nm) of the strained CPEPC-50 $\perp_z$ sample vs elongation (ϵ) and (b) the angle ϕ (deg) of the scattering maxima with respect to the meridian vs elongation (ϵ) mesaured from 2D-SAXS pattersn show in Figure 5.

of a $\perp_z$ CPC sample. Upon elongation past the sample yield point, the two-spot SAXS pattern in the q_y-q_z plane associated with the $\perp_z$-oriented morphology transforms into a four-spot pattern in the neck of the sample. The latter scattering pattern has been previously assigned to the chevron morphology, observed previously in aligned lamellar SBS[9] and EPE[17] samples as well as isotropic SBS[3,8] and SES[6] samples. $\perp_z$ CPC shows no discernible scattering pattern in the q_x-q_z plane (data not shown), also consistent with the chevron assignment. Chevron formation occurs only in the thinnest dimension of the sample ($\nabla\mathbf{v}$ direction), thus resulting in neck propagation only in the thinnest dimension of the sample or "one-dimensional necking".[10] As the sample is elongated, one observes that the azimuthal angle at which the scattering maxima occur increases monotonically until failure, with no discernible perturbation of the principal domain spacing of the block copolymer. A broadened two-spot pattern is observed upon failure and recovery, attendant with nearly complete macroscopic elastic recovery of the sample. $\perp_z$ CPCPC forms chevrons in a manner analogous to $\perp_z$ CPC; however, σ_{fail} for CPCPC is substantially larger than that for CPC with a comparable ϵ_{fail} (Figure 6, lower panels).

"In situ" SAXS patterns for an analogous tensile experiment with a $\perp_z$ CPEPC-50 sample are shown in Figure 7. $\perp_z$ CPEPC-50 also exhibits one-dimensional necking in the thinnest dimension of the sample. SAXS patterns of CPEPC-50 evolve as a function of elongation from the native two-spot pattern to a four-spot pattern, in which the azimuthal angle ϕ increases with elongation with no significant change in the domain spacing of the supramolecular lamellar structure (Figure 8a). A plot of the azimuthal angle as a function of the elongation (Figure 8b) shows that the chevron angle plateaus at $\phi \sim 76°$, comparable to that observed in $\perp_z$ CPC (Figure 6). Figure 9 displays the results of the WAXS analyses of CPEPC-50 during elongation and after failure. WAXS elucidates changes in the E crystal morphology and orientation within the CPEPC structure. Upon strain-induced chevron formation, the E crystal stems reorient toward the drawing axis. Azimuthal integrations of the SAXS and WAXS patterns in the q_y-q_z plane over constrained solid angles are shown in parts a and b of Figure 10, respectively, at $\epsilon = 3.5$ and upon failure and recovery. Integrations of the WAXS patterns show that the E crystallites cant ~9° away from the strain direction while the lamellar planes of the chevron are tilted 14° relative to the strain axis. Therefore, the E crystal stems are oriented at a 5° angle relative to the microphase separated lamellar interfaces in the chevron. Upon failure, persistence of the chevron structure and E crystal orientation are consistent with the observed permanent set of the sample. Integrations of the SAXS and WAXS patterns of the failed CPEPC-50 samples show that the E crystallites remain tilted by 6° with respect to the lamellar interfaces of the chevron morphology (Figure 10).

In contrast to $\perp_z$ CPEPC-50 and other members of this series of materials, the $\perp_z$ CEC exhibits brittle fracture at low strains with no observable change in the microdomain structure by SAXS. The CEC samples show no evidence of yielding before fracture, although the brittleness of samples renders these samples difficult to study. These data are consistent with a previous report,[4] although the strain at failure is slightly higher as noted earlier.

Microstructural Investigations of $\perp_x$ Samples. SAXS and WAXS analysis of $\perp_x$ CPEPC samples undergoing uniaxial deformation reveals a different evolution of the microstructure and the E crystal morphology as compared to $\perp_z$ CPEPC. SAXS patterns in the q_z-q_x plane of the deformed region of a representative CPEPC-70 sample at various elongations are shown in Figure 11. The lamellar domain spacing of $\perp_x$ CPEPC-70 initially contracts upon application of strain, evidenced by the increase in $|q^*|$ and the broadening of the scattering maxima. Complete disruption of the lamellar structure ensues upon yielding and subsequent drawing of the sample. As the sample strain hardens, the appearance of a pair of broad, horizontal scattering maxima suggests a lack of long-range order in the sample. Upon failure and elastic recovery, SAXS patterns of the relaxed samples exhibit a "cross" pattern, suggesting a preferred lamellar orientation with respect to the strain axis. WAXS analysis of the failed and recovered samples confirms the reorientation of the E crystal stems along the strain direction.

Properties of the CEC/CPC-50 Blend. Since the presence of rubbery P blocks in the $\perp_z$ CPEPC materials renders them ductile as compared to the brittle glassy−semicrystalline $\perp_z$ CEC, we investigated the possibility of mitigating the brittleness of $\perp_z$ CEC and enhancing its toughness by blending with CPC. Since the interaction parameter χ_{EP} between the E and P blocks is small and the E and P block molecular weights are substantially smaller than those required to achieve melt phase separation,[31,36] we anticipated the miscibility of a blend of CPC and CEC at matched segregation strengths. Equal masses of CEC and CPC were blended by dissolution in benzene as a common solvent followed by solvent removal by freeze-drying at 22 °C, such that the resulting CEC/CPC blend had $w_E \sim w_P$ to facilitate comparison with CPEPC-50. As in the case of the CPEPC materials in which the E and P blocks are covalently linked and phase mixed in the melt due to the small magnitude of χ_{EP}, we expected the CEC/CPC-50 blend to adopt an ordered lamellar melt morphology comprised of alternating stacks of C and mixed E/P microdomains due to the chemical incompatibility of the C and E/P segments.[28] Upon cooling these melts, vitrification of the C domains enforces the lamellar morphology within which templated E crystallization occurs. The latter event causes a crystallization-induced segregation of the E blocks from the amorphous P segments within the lamellar microdomains.

The phase behavior, morphology, and thermal properties of CEC/CPC-50 were examined in detail. Dynamic mechanical spectroscopy[31,32] indicates the presence of a single order−disorder transition temperature $T_{ODT} = 225$ °C (Figure 12a), located between those of the constituent CEC and CPC. Synchrotron SAXS of the blend reveals a well-formed lamellar morphology having a single principal domain spacing $d = 22$

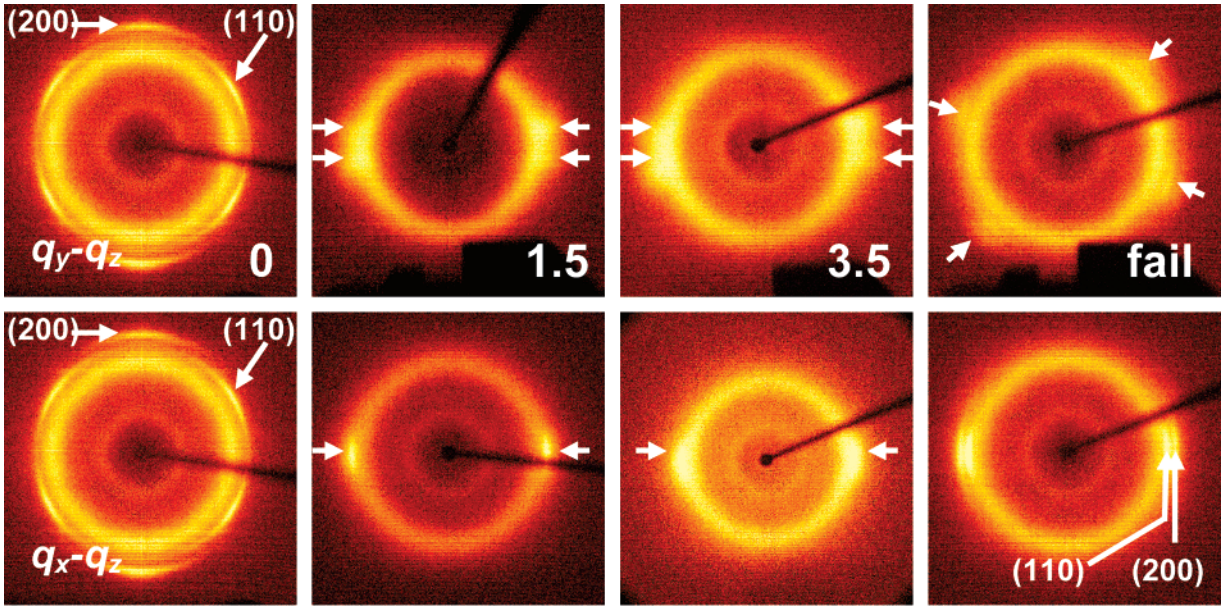

Figure 9. Representative "in situ" WAXS patterns taken with the X-ray beam incident on the q_y-q_z and q_x-q_z planes during tensile deformation of a $\perp_z$ CPEPC-50 sample at the indicated elongation (ϵ) and after failure and recovery. Measurements reflect the structure in the necked region of the specimen.

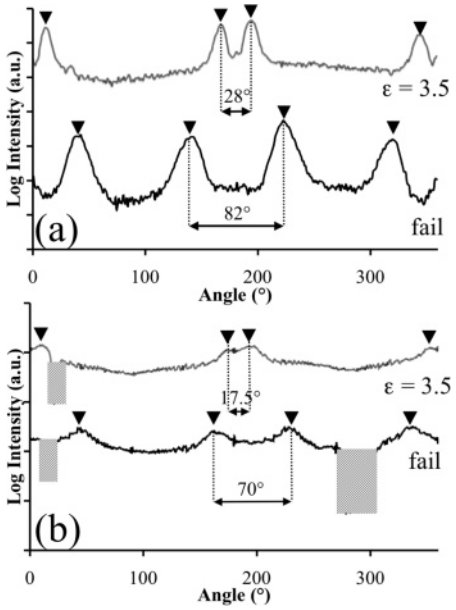

Figure 10. Azimuthal integrations of (a) 2D-SAXS patterns taken at $\epsilon = 3.5$ and after failure and recovery with 0.026 Å$^{-1} \leq q \leq$ 0.035 Å^{-1}, and (b) 2D-WAXS patterns taken at $\epsilon = 3.5$ and after failure and recovery with 1.80 Å$^{-1} \leq q \leq$ 2.02 Å^{-1} (the shaded boxes cover minima due to shadows cast by the sample mount and beam stop stem as seen in Figure 9).

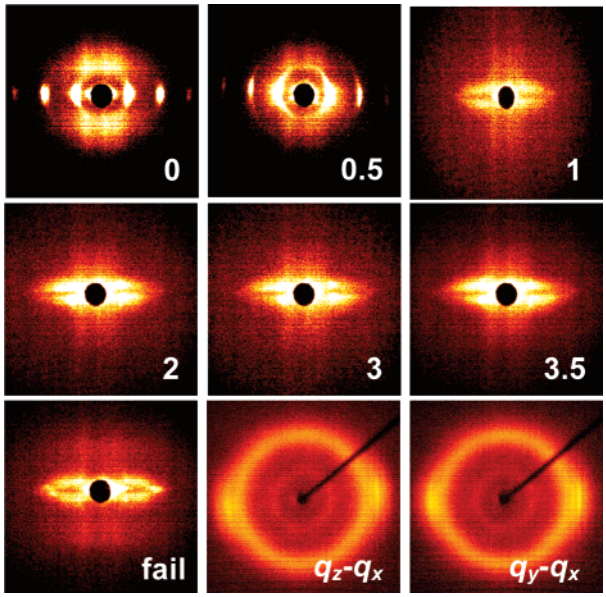

Figure 11. Representative "in situ" SAXS patterns (top) taken with the X-ray beam incident on the q_z-q_x plane during tensile deformation of a $\perp_x$ CPEPC-70 sample at the indicated elongation (ϵ) and after failure and recovery, along with corresponding WAXS patterns of sample after failure and recovery taken with the X-ray beam incident on the q_z-q_x and q_y-q_x planes (right two panels in the bottom row).

nm (Figure 12b,c), which compares favorably to the weighted average of the *d*-spacings of the blend components. In accord with our previous report on CPEPC materials, the diminished intensity of the $3q^*$ scattering maximum is attributed to the fact that $f_C \sim 0.41$, and the electron densities of the E and P blocks are comparable in the melt at 150 °C. SAXS analysis verified the location of T_{ODT}, as evidenced by the dissolution of higher order scattering peaks to yield correlation-hole scattering above T_{ODT}.[37] In contrast to the previously reported SAXS patterns of the CPEPC materials at 22 °C, the scattering pattern associated with CEC/CPC-50 does not exhibit substantial negative concavity due to E crystallization. DSC analysis revealed that the peak melting temperature of the semicrystalline E block of the blend is the same as that of the parent CEC ($T_{m,E}$ = 94.2 °C), with a comparable crystallinity X_c in the E block and overall crystallinity to CPEPC-50. The slightly depressed melting temperature for CPEPC-50 of $T_{m,E}$ = 92.8 °C indicates a reduced E crystal thickness in the pentablock copolymer.[38]

Reciprocating shear processing of the blend under the established protocol resulted in well-oriented samples, from which $\perp_z$ tensile samples were cut. The CEC/CPC-50 blend samples exhibit slightly enhanced mechanical properties as compared to CPEPC-50, primarily a ~40% increase in the failure stress (Table 2). The elastic modulus and yield stress for the blend are slightly lower than those observed for CPEPC-50. "In situ" SAXS analysis of the deformed tensile samples reveals chevron formation upon yielding, with only partial

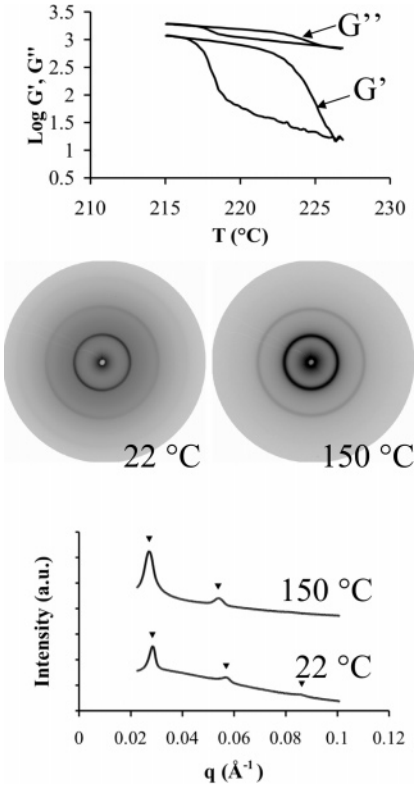

Figure 12. (a) Isochronal temperature ramp data at $\omega = 1$ rad/s and $|\gamma| = 1\%$ for the CEC/CPC-50 blend indicating a large drop in G' and G'' at $T_{ODT} = 225$ °C associated with the order−disorder transition temperature. (b) Two-dimensional synchrotron SAXS patterns of CEC/CPC-50 blend at 22 and 150 °C, and (c) azimuthal integrations of these scattering patterns consistent with a lamellar morphology.

chevron recovery upon failure and recovery of the sample akin to that observed for CPEPC-50 (data not shown).

Discussion

Properties of the $\perp_z$ Samples. Analyses of the $\perp_z$ samples provide unique insights into the effects of block copolymer composition on the mechanical properties of the CPEPC polyolefins, particularly the incorporation of a rubbery P block into the glassy−semicrystalline C/E multiblock copolymers. As in the case of the polydomain materials in which the lamellar grains are not preferentially oriented, the $\perp_z$-oriented CPEPC and CPC tensile samples exhibit increased ductility as the E content decreases with comparable engineering failure stresses.[28] The $\perp_z$ CEC, however, exhibits brittle fracture at low strains consistent with previous observations.[4] Phatak et al. recently explained the brittleness of $\perp_z$ CEC by examining the relative magnitude of the critical resolved shear stress required for deformation of E crystallites within the semicrystalline domains relative to the yield stress required for buckling and grain rotation in the more ductile CECEC copolymers.[5] If the critical resolved shear stress to deform the E crystals is greater than the yield stress of the sample, straining the samples results in brittle fracture in the C domain. Furthermore, the macroscopic alignment of the lamellae allows cracks in the C domains to easily propagate through the material resulting in catastrophic failure of the tensile samples.

The CPEPC materials, however, accommodate strain by virtue of the compliance imparted by the low-modulus P blocks, such that the layers can dilate slightly and access a critical strain at which buckling occurs to form the chevron morphology.[16] Upon chevron formation, $\perp_z$ CPEPC accommodates further strain at a constant stress by decreasing the chevron angle between the layers whereby each undulation in the layers effectively acts as a microscopic hinge. Chevron formation notably occurs with constant domain spacing as previously reported for aligned lamellae-forming SBS triblocks, a condition that necessarily implies that the layers must break, dilate, and shear past each other in a process termed "affine rotation".[9] Consistent with the notion that the resistance to affine rotation originates from shearing of the E domains is the observation that both the elastic moduli and the yield stress increase monotonically as a function of the E content in CPEPC. The previously noted increase in E crystal thickness (evidenced by higher E block melting temperatures with increasing w_E) helps to account for the increased stress required for plastic deformation at higher E contents, since the yield stress of E homopolymer is known to depend on crystallite size.[38] The nonlinear increase in the elastic modulus E as a function of w_E may be attributed to the physical cross-linking of polymer chains through interchain cocrystallization and changes in the entanglement densities in the E and P blocks. The shear component of the affine rotation in CPEPC likely leads to a shear-induced recrystallization of the semicrystalline E domains as opposed to a simple reorientation of these crystallites along the strain direction.[39,40]

Geometric calculations of the expected elongation at a given chevron angle ($\epsilon = d/\cos\phi$) under the affine rotation model agree quite well with the observed results as was previously observed for $\perp_z$-oriented SBS triblock copolymers.[9] Not surprisingly, the extensibility of the CPEPC materials depends in large part upon the composition such that low P content leads to lower extensibility. This observation may reflect the ability of entanglements in the P block to easily slip and delay the onset of defect activation and ultimate failure, whereas the number of amorphous entanglements in the E block may be decreased by crystallization thus decreasing its load bearing capability. The load bearing ability of the E block is likely reduced by the fact that these entanglements are pinned by the E crystallites in a size-dependent manner. Given that the overall crystallinity in the CPEPC series is constant, the density of load bearing entanglements in the PEP segment may increase as $\xi \rightarrow 0$.

In contrast to the polydomain CPEPC samples, the E crystallites in the $\perp_z$-samples do not simply orient with the crystal stems aligned with the applied strain axis upon affine rotation of the broken lamellar grains. WAXS analysis shows that the crystallites instead cant at 9° relative to the strain axis or 5° relative to the microphase separated lamellar interfaces of the chevron texture, a value that increases slightly to 6° upon failure and relaxation. This observation leads us to speculate that the shear component of the tensile stress prevents the crystallites from aligning along the strain axis and instead causes the crystal stems to tilt away from the strain axis, as shown in Figure 13. This shearing action likely results in an E crystal morphology in which the crystalline fold surface forms an acute angle relative to the chain axis, a morphology previously observed in solution-crystallized polyethylenes.[43] By virtue of the changes in the E crystal morphology which establish a new configuration of physical cross-links in the PEP segment, the chevron texture is retained upon failure and permanent set is observed in the material. The expected permanent set calculated from the d-spacing and the chevron angle concur with the experimentally observed values. Note that this permanent set due to shear-induced recrystallization enables the production of high strength fibers by cold-drawing of CPEPC materials as previously reported.[28]

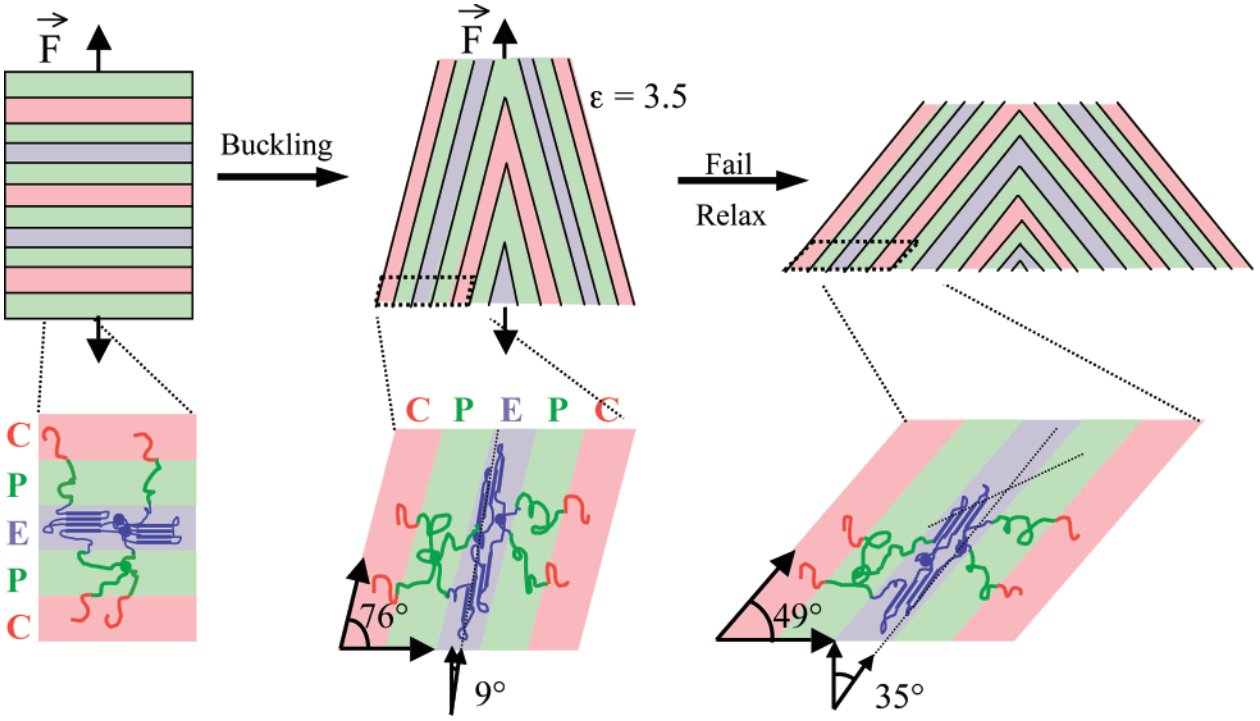

Figure 13. Proposed morphological changes in CPEPC-50 $\perp_z$ oriented tensile bars under tension deduced from SAXS and WAXS data shown in Figures 8 and 9, in which a buckling instability occurs to yield a "chevron" morphology. The lamellar planes of the microphase-separated structure tilt at a 14° angle from the strain direction at $\epsilon = 3.5$, within which the E crystallites are oriented at a 9° with respect to the strain direction. Upon failure of the sample and subsequent recovery, the sample retains a chevron structure consistent with the macroscopic permanent set. In the deformed sample, the microphase-separated interfaces tilt at a 51° angle from the strain direction, within which the E crystallites are canted 35° from the strain axis. Note that the shearing of the layers in the deformed samples may result in the E crystal fold surfaces forming an acute angle with the chain axes, as depicted (lower right).

The engineering stresses at failure (σ_{fail}) for all of the CPEPC materials are comparable, implying a common failure mechanism. At low strains, the C domains act as glassy plates such that elastic and plastic deformation occurs in the P and E domains. Upon shear-induced recrystallization of the E to form crystallites oriented toward the strain direction, the brittle C domains become the weak link in these materials. Since the molecular weight of the C blocks in the CPEPC materials is much smaller than the entanglement molecular weight M_e(C) $\sim$ 40 kDa, chain pullout from the C domains is presumed to be the mechanism of ultimate failure.[24,41] Therefore, ultimate failure is expected when either the normal stress or the shear stress on the C domains exceeds its fracture stress. The applied tensile force on a chain relative to the interface between the C and the E/P microdomains can be resolved into a true normal stress $N_{true,fail} = \sigma_{true,fail} \cos^2 \phi$ and a true shear stress $\tau_{true,fail} = \sigma_{true,fail} \cos \phi \sin \phi$,[42] where ϕ is the observed azimuthal angle of the chevron in the 2D-SAXS pattern and the true stress is given by $\sigma_{true,fail} = \sigma_{fail}(\epsilon_{fail} + 1)$ assuming an affine deformation. Using the experimental values for ultimate properties and ϕ determined from SAXS, we find that $N_{true,fail} \sim 3-4$ MPa and $\tau_{true,fail} \sim 14-16$ MPa at failure for all CPEPC materials (Table 4). This suggests that the maximum normal stress is comparable to stress required for chain pullout, which is consistent with the extreme brittleness of low molecular weight C homopolymer. This calculation does not hold in the case of the pentablock copolymer CECEC in which individual extended chain conformations span (stitch together) up to five lamellar domains to provide improved toughness as compared to CEC triblock copolymer.[4] The data presented herein indicate that the CPCPC pentablock exhibits enhanced mechanical properties as compared to the CPC triblock as a consequence of the bridging conformations available to the pentablock copolymer. On this basis, we expect that the nonablock CPEPCPEPC would have enhanced mechanical strength comparable to the CPCPC and CECEC pentablock copolymers.

Table 4. $\perp_z$ CPEPC True Stress ($\sigma_{true,fail}$), Critical Resolved Shear Stress (τ), and Normal Stress (N) at Failure[a]

sample	chevron angle ϕ (deg)[b]	$\sigma_{true,fail}$ (MPa)[c]	τ (MPa)[d]	N (MPa)[e]
CEC	n.a.	16.5	n.a.	n.a.
CPEPC-70	76.0	60.1	14.1	3.52
CPEPC-50	76.0	62.8	14.7	3.67
CPEPC-30	78.0	78.0	15.9	3.37
CPC	79.5	89.4	16.0	2.96
CECCPC-50	n.d.	93.0	n.a.	n.a.
CPCPC	78.0	130.2	26.5	5.63

[a] All calculations assume an affine deformation. [b] ϕ measured by SAXS before failure. [c] $\sigma_{true,fail} = \sigma_{fail}(\epsilon_{fail} + 1)$. [d] $\tau = \sigma_{true,fail} \sin \phi \cos \phi$. [e] $N = \sigma_{true,fail} \cos^2 \phi$.

Properties of the $\perp_x$ Samples. The mechanical response of the $\perp_x$ CPEPC differs substantially from that of the $\perp_z$ CPEPC, since the applied load is distributed across the glassy, rubbery, and semicrystalline domains simultaneously. Consequently, the initially observed yielding and subsequent plastic deformation must involve fracture of the glass into plates of varying sizes within an elastomeric matrix as in the case of the analogous SBS sample.[9] Again the monotonic increases in the elastic modulus E and the yield stress σ_{yield} as a function of ξ reflect the dependence of these quantities on the E crystallite thickness and the amorphous entanglement densities of the PEP blocks. As a consequence of the fracture of the glass, the samples unevenly rupture along the lamellar interfaces to form macroscopic strands that tear unevenly and prevent observation of any obvious trends in the ultimate mechanical properties. SAXS analysis corroborates the destruction of the ordered microdomain

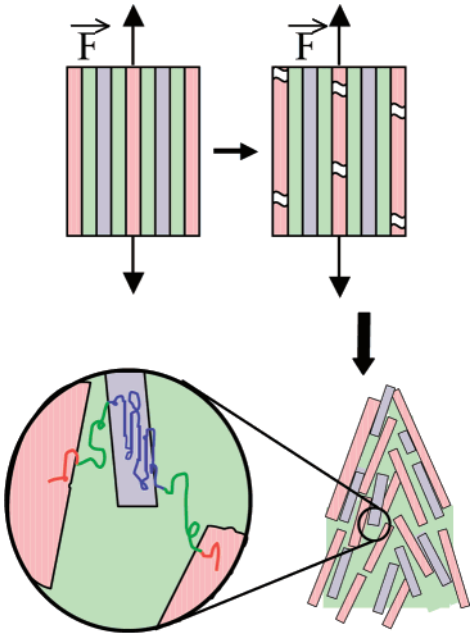

Figure 14. Proposed deformation mechanism in $\perp_x$ CPEPC materials. The initial mechanical response reflects that of the load bearing C domains (red), which fracture thereby allowing the rubbery P (green) and semicrystalline E (blue) domains to plastically deform. Ultimately, the glassy lamellae align along the strain direction with some distribution of sizes and lamellar spacings to permit the observed maximum tensile deformation.

structure by virtue of the brittle fracture of the glass, as evidenced by the pair of broad horizontal scattering maxima (Figure 11). Chain deformation by virtue of the applied load causes the glassy plates to align into a poorly ordered "chevron-like" morphology schematically depicted in Figure 14. This leads to the "cross" pattern observed by SAXS upon failure and elastic recovery of the sample. The similarity in the mechanical response of the polydomain CPEPC and the $\perp_x$ CPEPC can be rationalized on the basis of recent work by Phatak et al., in which the mechanical properties of the polydomain sample were shown to reflect the composite properties of the randomly oriented lamellar grains with a dominant contribution from grains oriented toward the $\perp_x$ direction.[5]

Toughening CEC by Addition of CPC. Since the CEC and CPC triblock copolymers have matched segregation strengths and the interaction parameter between E and P is small enough to render the low molecular weight E and P blocks miscible, the CEC/CPC-50 blend exhibits a single domain spacing and order−disorder transition temperature. Shear processing this blend yields well-oriented samples, which were studied only in the $\perp_z$ orientation. The observed properties of CEC/CPC-50 mimic those of $\perp_z$ CPEPC-50 with a slightly lower yield stress σ_{yield} and a higher ultimate failure stress σ_{fail}. This experiment demonstrates that the mechanical properties of CEC can be modulated by introducing compliance into the material by either: (i) constructing pentablock copolymers in which a soft P block buffers the C/E interface or (ii) blending the amorphous CPC material into CEC. These strategies complement the previously described toughening strategy introduced by Mori et al., in which CECEC pentablock copolymer was blended with CEC in order to enhance the toughness of the CEC $\perp_z$ oriented tensile samples.[26] Significantly, the nearly identical mechanical responses of CPEPC-50 and CEC/CPC-50 reinforce the notion that the overall entanglement density of the soft domains plays a central role in establishing the failure stress.[27]

Conclusion

Herein we have described the anisotropic mechanical properties of shear processed lamellae-forming block copolymers comprised of glassy C, rubbery P, and semicrystalline E components in order to provide further insight into the previously reported properties of these materials. The results demonstrate that the application of a tensile load perpendicular to the layered microdomain structure in a glassy−semicrystalline C/E block copolymer results in brittle fracture at low strains. The addition of a rubbery P component to the lamellar structure as in the CPEPC pentablock copolymers provides a stress accommodation mechanism that results in buckling of the stratified structure at small strains and formation of a chevron morphology. Within the chevron structure, shear-induced recrystallization gives rise to a unique E crystal morphology in which the crystallites are not oriented rigorously along the strain axis, by virtue of a combination of tensile and shear forces. This new crystal morphology results in the ability to cold-draw these materials with a substantial amount of permanent set, which yields high strength fibers as reported in our earlier work.[28] Since the mechanism of failure in these materials is presumed to be chain pullout in the C domains, application of a simple mechanical model demonstrates that these materials fail once the normal stress on the canted C layers exceeds ~4 MPa. The observation that such a weak glassy C block coupled to semicrystalline E and rubbery P blocks can yield high strength materials demonstrates that entanglements in the PEP segment operate as a system of molecular pulleys, which distribute a large tensile load across the material in a manner analogous to a "block and tackle". These systematic studies establish that the mechanical response of C/E block copolymers can be subtly tuned by judicious incorporation of an elastomeric P segment. Alternatively, careful design and blending of glassy−semicrystalline CEC and glassy−amorphous CPC triblock copolymers yields materials exhibiting a composite mechanical response that mimics that of the three monomer CPEPC pentablock copolymers.

Acknowledgment. The authors gratefully acknowledge financial support from the Department of Energy through a subcontract to UT-Battelle (No. 4000041622), and the National Science Foundation Materials Research Science and Engineering Center (NSF-MRSEC) at the University of Minnesota (NSF DMR-0212302), and Medtronic Corp. This research made extensive use of NSF-MRSEC supported characterization facilities at the University of Minnesota. Portions of this work were performed at the DuPont−Northwestern−Dow Collaborative Access Team (DND-CAT) Synchrotron Research Center located at Sector 5 of the Advanced Photon Source (Argonne, IL). DND-CAT is supported by the E.I. DuPont de Nemours & Co., the Dow Chemical Co., and the NSF (DMR-9304725). Use of the Advanced Photon Source was supported by the U.S. Department of Energy, Office of Basic Energy Sciences, under Contract W-31-109-Eng-38. The authors also thank Alhad Phatak for stimulating discussions.

References and Notes

(1) Holden, G.; Legge, N. R.; Quirk, P. R.; Schroeder, H. E. In *Thermoplastic Elastomers*, 2nd ed.; Hanser/Gardner Publications: Cinncinati, OH, 1996; pp 47−70.
(2) Morton, M.; McGrath, J. E.; Juliano, P. C. *J. Polym. Sci., Part C* **1969**, *26*, 99−115.
(3) Kawai, H.; Hashimoto, T.; Miyoshi, K.; Uno, H.; Fujimura, M. *J. Macromol. Sci., Phys.* **1980**, *B17*, 427−472.
(4) Hermel, T. J.; Hahn, S. F.; Chaffin, K.; Gerberich, W. W.; Bates, F. S. *Macromolecules* **2003**, *36*, 2190−2193.

(5) Phatak, A.; Lim, L. S.; Reaves, C. K.; Bates, F. S. *Macromolecules* **2006**, *39*, 6221−6228.
(6) Séguéla, R.; Prud'homme, J. *Macromolecules* **1981**, *14*, 197−202.
(7) Pakula, T.; Saijo, K.; Kawai, H.; Hashimoto, T. *Macromolecules* **1985**, *18*, 1294−1302.
(8) Fujimura, M.; Hashimoto, T.; Kawai, H. *Rubber Chem. Technol.* **1978**, *51*, 215.
(9) Cohen, Y.; Albalak, R. J.; Dair, B. J.; Capel, M. S.; Thomas, E. L. *Macromolecules* **2000**, *33*, 6502−6516.
(10) Cohen, Y.; Thomas, E. L. *Macromolecules* **2003**, *36*, 5265−5270.
(11) Hartsock, D. L.; Stacy, N. E. In *Modern Styrenic Polymers: Polystyrene and Styrenic Copolymers*; Scheirs, J., Priddy, D. B., Eds.; John Wiley & Sons Ltd.: New York, 2003; pp 501−530.
(12) Mortensen, K.; Almdal, K.; Bates, F. S.; Koppi, K.; Tirrell, M.; Norden, B. *Physica B* **1995**, *213&214*, 682−4.
(13) Koppi, K. A.; Tirrell, M.; Bates, F. S. *Phys. Rev. Lett.* **1993**, *70*, 1449−52.
(14) Chen, Z.-R.; Kornfield, J. A. *Polymer* **1998**, *39*, 4679−4699.
(15) Honeker, C. C.; Thomas, E. L. *Chem. Mater.* **1996**, *8*, 1702−1714.
(16) Read, D. J.; Duckettm, R. A.; Sweeney, J.; Mcleish, T. C. B. *J. Phys. D: Appl. Phys.* **1999**, *32*, 1381.
(17) Koo, C. M.; Hillmyer, M. A.; Bates, F. S. *Macromolecules* **2006**, *39*, 667−677.
(18) Hucul, D. A.; Hahn, S. F. *Adv. Mater.* **2000**, *12*, 1855−1858.
(19) Bates, F. S.; Fredrickson, G. H.; Hucul, D. A.; Hahn, S. F. *AIChE J.* **2001**, *47*, 762−765.
(20) Patel, R. M.; Hahn, S. F.; Esneault, C.; Bensason, S. *Adv. Mater.* **2000**, *12*, 1813−1817.
(21) Vigild, M. E.; Chu, C.; Sugiyama, M.; Chaffin, K.; Bates, F. S. *Macromolecules* **2001**, *34*, 951−964.
(22) Cochran, E. W.; Bates, F. S. *Macromolecules* **2002**, *35*, 7368−7374.
(23) Ruokolainen, J.; Fredrickson, G. H.; Kramer, E. J.; Ryu, C. Y.; Hahn, S. F.; Magonov, S. N. *Macromolecules* **2002**, *35*, 9391−9402.
(24) Ryu, C. Y.; Ruokolainen, J.; Fredrickson, G. H.; Kramer, E. J. *Macromolecules* **2002**, *35*, 2157−2166.
(25) Hermel, T. J.; Wu, L.; Hahn, S. F.; Lodge, T. P.; Bates, F. S. *Macromolecules* **2002**, *35*, 4685−4689.
(26) Mori, Y.; Lim, L. S.; Bates, F. S. *Macromolecules* **2003**, *36*, 9879−9888.
(27) Lim, L. S.; Harada, T.; Hillmyer, M. A.; Bates, F. S. *Macromolecules* **2004**, *37*, 5847−5850.
(28) Mahanthappa, M. K.; Lim, L. S.; Hillmyer, M. A.; Bates, F. S. *Macromolecules* **2007**, *40*, 1585−1593.
(29) Phatak, A.; Macosko, C. W.; Bates, F. S.; Hahn, S. F. *J. Rheol.* **2005**, *49*, 197−213.
(30) Brandrup, J., Immergut, E. H., Eds.; *Polymer Handbook*, 3rd ed.; Wiley: New York, 1989.
(31) Rosedale, J. H.; Bates, F. S. *Macromolecules* **1990**, *23*, 2329−38.
(32) Rosedale, J. H.; Bates, F. S.; Almdal, K.; Mortensen, K.; Wignall, G. D. *Macromolecules* **1995**, *28*, 1429−43.
(33) Koppi, K.; Tirrell, M.; Bates, F. S.; Almdal, K.; Mortensen, K. *J. Rheol.* **1994**, *38*, 999−1027.
(34) Wu, L.; Lodge, T. P.; Bates, F. S. *Macromolecules* **2006**, *39*, 294−299.
(35) Wu, L.; Lodge, T. P.; Bates, F. S. *J. Rheol.* **2005**, *49*, 1231−1252.
(36) Maurer, W. W.; Bates, F. S.; Lodge, T. P.; Almdal, K.; Mortensen, K.; Fredrickson, G. H. *J. Chem. Phys.* **1998**, *108*, 2989−3000.
(37) Bates, F. S. *Macromolecules* **1985**, *18*, 525−8.
(38) Bassett, D. C. *Principles of Polymer Morphology;* Cambridge University Press: New York, 1981.
(39) Galeski, A. *Prog. Polym. Sci.* **2003**, *28*, 1643−1699.
(40) Seguela, R. *J. Macromol. Sci., Polym. Rev.* **2005**, *C45*, 263−287.
(41) Zhao, J.; Hahn, S. F.; Hucul, D. A.; Meunier, D. M. *Macromolecules* **2001**, *34*, 1737−1741.
(42) Calister, W. D. *Materials Science and Engineering: An Introduction*, 5th ed.; John Wiley & Sons: New York, 2000; p 160.
(43) Schultz, J. *Polymer Materials Science;* Prentice Hall: Englewood Cliffs, NJ, 1974; pp 30−39.

MA071196R